Unravelling the complexities of inorganic and supramolecular self-assembly in solution with electrospray and cryospray mass spectrometry

Haralampos N. Miras,† Elizabeth F. Wilson† and Leroy Cronin*

Received (in Cambridge, UK) 3rd November 2008, Accepted 5th January 2009
First published as an Advance Article on the web 13th February 2009
DOI: 10.1039/b819534j

Electrospray (ESI) and cryospray mass spectrometry (CSI-MS) are proving to be exceptionally versatile tools when used in conjunction with high resolution time-of-flight (TOF) systems to investigate the self-assembly of supramolecular architectures, inorganic coordination and organometallic compounds, labile molecules and clusters both from a structural and mechanistic point of view. In this feature article, we review very recent progress where mass spectrometry is being applied to highly labile and complex coordination and polyoxometalate (POM) cluster systems and we present some highlights from our initial electrospray and cryospray studies, which probe the self-assembly of inorganic cluster architectures. We discuss the major contributions of ESI and CSI-MS to labile and self-assembling inorganic architectures with great emphasis on future potential and ramifications for inorganic chemistry and the area of self-assembly as a whole.

1. Introduction

Molecular self-assembly is an interesting phenomenon since it governs how labile or supramolecular systems[1] are constructed from simple building blocks spontaneously into complex architectures.[2] Such self-assembly processes are highly dependent upon the reaction conditions,[3] often to such a degree that total control is never easily achieved.[4]

Many researchers have capitalized on the unexpected architectures produced in the effort to design, often with well-defined building blocks, new architectures and materials that exhibit fundamentally new and interesting properties as a result of the self-assembly process.[5] The serendipitous result is often used as a bootstrap to control the formation of related architectures in further work.[6] In our research we have focused on the self-assembly of polynuclear coordination compounds[7] and of polyoxometalate clusters.[8,9] For both classes of materials, it is a great challenge to understand the self-assembly since conventional spectroscopic techniques have significant drawbacks. For example, NMR is of limited use when the symmetry of the assembling architecture is high,[10] when the structures are labile or paramagnetic, and for nuclei that

WestCHEM, Department of Chemistry, The University of Glasgow, Glasgow, Scotland, UK G12 8QQ.
E-mail: L.Cronin@chem.gla.ac.ukhttp://www.chem.gla.ac.uk/staff/lee; Fax: +44 (0)141 330 4888
† Both of these authors contributed equally to this article.

Haralampos N. Miras

Haralampos N. Miras gained his BSc degree and PhD under the supervision of Prof. T. A. Kabanos at Ioannina University in 2004. In 2005 he took up a post doctoral fellowship with Prof. R. G. Raptis (University of Rio Piedras, Puerto Rico, USA) in pyrazolate-based coordination materials. In September 2006 he took up a research associate position in the group of Prof. L. Cronin at the University of Glasgow in Scotland, UK in the area of discovery, synthesis and mechanistic studies using ESI–CSI-MS of large polyoxometalate and coordination clusters. His research interests focus on polyoxometalate and coordination chemistry.

Elizabeth F. Wilson

Elizabeth F. Wilson was born in Somerset, UK. She gained her MChem(hons) degree in chemistry from the University of York and is currently studying for her PhD under the supervision of Prof. L. Cronin at the University of Glasgow. Her research interests are in the application of mass spectrometry to inorganic systems, polyoxometalate synthesis, and inorganic–organic hybrid materials.

have a poor receptivity. In this feature article, we will explore very recent results from utilizing high resolution time-of-flight (TOF) mass spectrometry to examine the structures and assembly–disassembly of high nuclearity polyoxometalates[11] and coordination clusters.[12–14] Further, we will start to explore how temperature-controlled mass spectrometry can give unprecedented information regarding the kinetics and number of species present, and help validate the identity of the transmitted ions in the gas phase and their relationship with the parent ions present in solution.

In all these respects polyoxometalate and coordination clusters represent excellent model systems and will be briefly introduced here. Polyoxometalate (POM) chemistry is one of the most diverse and rapidly expanding areas in inorganic chemistry today,[8,9,11] and the ongoing interest in the field is highlighted by the large and diverse number of new iso- and heteropolyoxometalate clusters that have been discovered in recent years.[8,9,11] This diversity in the architecture of POM-based clusters is revealed by a huge variety of shapes, sizes and compositions, from small (*e.g.* $[Mo_6O_{19}]^{2-}$)[15a–c] to nanosized species (*e.g.* $[H_xMo_{368}O_{1032}(H_2O)_{240}(SO_4)_{48}]^{48-}$, $\{Mo_{368}\}$), all of which are formed under "one-pot" reaction conditions, see Fig. 1.[16]

Owing to their sizes, structures, and properties (catalytic, redox,[17–20] photochemical, and even biological activity[21] *etc.*), POMs are often referred to as highly functional, soluble metal-oxide fragments and are receiving considerable attention.[8,9,11,22–25] Polynuclear coordination compounds also represent a vast class of compounds that have been widely investigated from a fundamental, structure and bonding, as well as a physical properties development point of view.[7,13,14] Ligand design in polynuclear coordination chemistry has been used extensively in many areas, for example in assembly of reactive motifs for catalysis,[13c] bio-inorganic modelling,[13b] and new materials design. Despite the increasing interest in both polyoxometalate and polynuclear coordination clusters, the accurate determination of formulae and structure still represents a great challenge[8,9] vital for understanding cluster formation and their exploitation. Moreover, the controlled assembly of POM or complex-based building blocks defines a crucial challenge to link the building blocks, so they can assemble into pre-defined architectures. However, despite the increasingly intensive research in this area, progress in understanding the mechanisms of self-assembly that govern POM and multi-metallic coordination structure formation remains limited.[7–13,14] In practice, this lack of understanding leads to experimentation where manipulation of reaction parameters in the commonly used "one-pot" syntheses often leads to the formation of new structures, albeit *via* a somewhat serendipitous approach.[6,13,16a] Although the fundamental speciation process underlying the formation of low nuclearity molybdates and tungstates is well understood,[12c,d] the process by which larger or polymeric structures are formed is not clear due to the large library of building blocks, fragments, and clusters potentially available as the number of building blocks increases.[23] Thus, there is a clear need to develop approaches to bridge the gap between solid-state and solution studies[8c,26] so that the mechanism of self-assembly can be explored in a more systematic way.

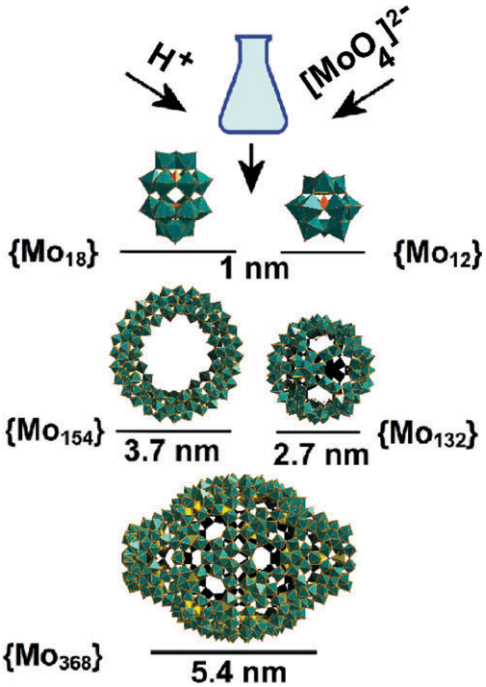

Fig. 1 Self-assembly of polyoxometalate clusters from $\{Mo_{12}\}$[15d] to the protein-sized $\{Mo_{368}\}$.[16a] The Mo centres are shown as green polyhedra.

Therefore, given the enormous challenge of following and understanding the self-assembly process for a range of cluster-based architectures, we set out to use electrospray (ESI) and cryospray mass spectrometry (CSI-MS), with a high resolution time-of-flight (TOF) detector, to identify novel species and investigate the self-assembly of labile, cluster-based and supramolecular systems in solution.[26]

2. Background on ESI-MS studies of POMs

ESI-MS has been used extensively to investigate many types of polyoxometalates including vanadates,[26] niobates,[27] tantalates,[28] chromates,[28] molybdates,[29] tungstates,[30–33] and rhenates.[34] Howarth *et al.* investigated aqueous solutions of isopolytungstates,

Lee Cronin

Lee Cronin graduated from York in 1994 (BSc.) and 1997 with a DPhil in bio-inorganic chemistry. He then took post doctoral fellowships in macrocyclic ligand design (University of Edinburgh, 1997) and large polyoxometalate clusters (University of Bielefeld, 1999) in the group of Prof. A. Müller. He started as a lecturer in 2000 at the University of Birmingham, and in 2002 he moved to Glasgow and was promoted to Reader in 2005 and Professor in 2006. He has wide ranging research interests centred around synthesis of complex and large chemical architectures as well as an interest in chemical complexity and self-organization in chemical systems.

peroxotungstates, and heteropoly-molybdates, detecting the $[W_6O_{19}]^{2-}$ and $[W_2O_7]^{2-}$ species in aqueous solution for the first time.[35] Mixed-metal heteropolyanion species were also investigated and the series of $[H_xPW_nMo_{12-n}O_{40}]^{(3-x)-}$ species reported. Further, it was shown that the ESI-MS-determined concentration of sensitive species (*i.e.* sensitive to changes in pH or the presence of other species) may differ from that determined in bulk measurements. Such studies have been extended to other clusters. For instance, it was shown that heteropolyoxomolybdate[36] compounds in acetonitrile could be successfully identified as intact anionic species, *e.g.* $[S_2Mo_{18}O_{62}]^{2-}$. Also, mixed-metal polyoxomolybates and tungstates could be identified in solution,[37] and studies on isopolyoxomolybdates,[29] tungstates[38] and even isopolyoxochromates have been examined.[32] In each case, an aggregation process of additive polymerization involving $\{MoO_3\}$, $\{WO_3\}$ or $\{CrO_3\}$ moieties, respectively, was identified as giving rise to the larger POM aggregates observed.[29,32]

In addition, the wide applicability of the ESI-MS technique to complex systems and mixtures has been demonstrated in catalytic studies where the real time transformation of the substrate can be observed, helping the proposal of a mechanistic pathway.[39a,39b] Studies into the potential-dependent formation of unknown multinuclear and mixed-valence polyoxomolybdate complexes when using on-line electrochemical flow cell electrospray mass spectrometry (EC-ESI-MS) have also been presented.[39c]

2.1 Background to CSI-MS

Cryospray (also known as coldspray) mass spectrometry was developed by Yamaguchi *et al.*[40] in order to investigate unstable organometallic complexes in which the presence of weak, non-covalent interactions had precluded analysis by other ionization techniques such as fast atom bombardment (FAB), matrix assisted laser desorption ionization (MALDI), and electrospray ionization (ESI) due to dissociation of the species. The technique is, therefore, of interest for investigations of labile POM systems because previous ESI-MS studies of such systems have been limited by the use of low resolution detectors and the high temperatures utilized in the ESI process.

The cryospray source consists of, essentially, an electrospray source where the N_2 capillary and sprayer gases are maintained at very low temperatures (minimum −100 °C). The use of low temperature gases promotes ionization of the target molecules, not by desolvation as in the conventional ESI process, but by increasing the polarizability of the target molecules at low temperature (*i.e.* the result of higher dielectric constant at low temperature).[40] This allows the molecular ions of unstable species to be generated and transferred efficiently into the MS detector with minimal fragmentation effects.[40,41]

An example of the potential of CSI-MS to investigate weakly hydrogen-bonded organic aggregates is the observation of large, hydrogen-bonded, chain structures of amino acids in solution, *e.g.* L-serine, glycine, L-valine.[42] These observations are consistent with the single-crystal X-ray crystallographic data for some of these amino acids in the solid state. In this study, CSI-MS analysis also allowed observation of alkali metal ion mediated aggregation of L-proline into cyclic clusters composed of trimeric and tetrameric subunits.

The application of CSI-MS analysis to organometallic systems has not allowed only identification of organometallic complexes in solution,[40] but also clarification of molecular structures previously not possible using other analytical techniques such as NMR and single-crystal X-ray diffraction.[40] For example, the study of adamantanoid-type Pt(II) complexes by CSI-MS allowed confirmation of the numbers and structures of encapsulated guest molecules;[40,43] and the study of interlocking Pt(II) cage complexes composed of tris-(4,4′-bipyridyl)-1,3,5-triazine ligands allowed clarification of the interlocking behaviour of the ligand structures in solution and elucidation of the location of counter-anions.[40] CSI-MS has also been utilized in conjunction with NMR studies to investigate the metal-induced self-assembly in nitromethane of a resorcin[4]arene derivative coordinating Pd or Pt. The coexistence of an interclipped supramolecular capsule and intraclipped bowl in dynamic equilibrium was identified using these techniques.[44]

3. Application of high resolution ESI-MS and CSI-MS to polyoxometalate cluster systems

In the context of this article it is worth pointing out that POMs are ideal candidates for high resolution studies since they have complex isotopic envelopes resulting from the high number of stable isotopes of tungsten (^{182}W, 26.5%; ^{183}W, 14.3%; ^{184}W, 30.6%; ^{186}W, 28.4%) and molybdenum (^{92}Mo, 14.8%; ^{94}Mo, 9.3%; ^{95}Mo, 15.9%; ^{96}Mo, 16.7%; ^{97}Mo, 9.6%; ^{98}Mo, 24.1%; ^{100}Mo, 9.6%), and are intrinsically charged. This allows complete determination of the cluster formula down to the last proton by matching the calculated *vs.* experimentally obtained envelopes. The difficulty associated with determining the protonation state of the cluster has thus far been a major drawback of standard crystallographic XRD studies, which often do not provide direct information on the protonation state of the cluster anions. Therefore, mass spectrometry of polyoxometalates has the potential to become the standard analysis technique for complex cluster systems since it provides vital complementary information of the cluster composition in solution[45] which cannot be deduced from crystallographic studies, as shown by the following example.

3.1 Probing protonation *vs.* heteroatom inclusion with ESI

The rugby ball-shaped clusters $[H_mW_{18}O_{60}X_n]^{y-}$ (where X = As, Sb, Bi)[46–48] have been known for three decades, with an approximate formulation of $n = 1$, but their precise composition could not be confirmed unambiguously due to disorder of the heteroatoms over two positions in a single cluster. However by using ESI-MS, we recently reported that we were able to directly probe the D_{3d} symmetric isomer of the Sb-based heteropolyoxotungstate $[H_mSb_nW_{18}O_{60}]^{y-}$.[49] During the course of these studies,[9c] we discovered that the correct formulation is where the cluster contains one heteroion disordered over two positions (Fig. 2, LHS). This situation can be compared with the discovery of $[H_mP_nW_{18}O_{62}]^{y-}$, which was also reported with $n = 1$, see Fig. 2 (RHS). Both clusters appear to include only one heteroatom; in addition, the $[H_4Sb_1W_{18}O_{60}]^{7-}$ is templated by a pyramidal SbO_3^{3-} anion whereas $[H_4P_1W_{18}O_{62}]^{7-}$ contains one tetrahedral PO_4^{3-} anion. ESI-MS results were obtained on

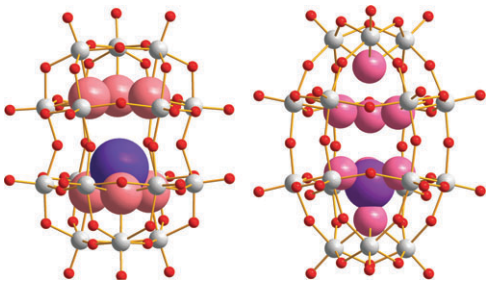

Fig. 2 Representation of the structures of $[H_4Sb_1W_{18}O_{60}]^{7-}$ and $[H_5P_1W_{18}O_{62}]^{7-}$. Colour scheme – W: grey; O: red; Sb and P: purple.

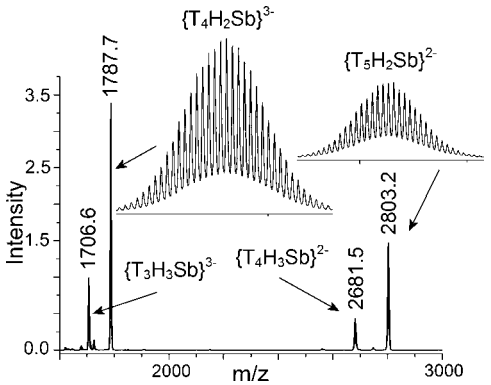

Fig. 3 The negative ion mass spectrum of the Sb-containing cluster showing the series of tri- and tetra-protonated forms of $(TBA)_y[H_xSb_1W_{18}O_{62}]^{(9-(x+y))-}$. T = TBA^+, Sb = $Sb_1W_{18}O_{60}$ (intensity × 10^4).

tetrabutylammonium salts of the clusters in acetonitrile solution, see Fig. 3 and 4.

The cation-exchange process was used because the TBA^+ cations have a much higher mass than Na^+ or K^+ and give a larger separation between signals corresponding to differently charged or protonated cluster states. Exhaustive analysis of the ESI-MS data shows that the compounds can be unambiguously identified in both positive and negative ion modes and $[H_mSb_nW_{18}O_{60}]^{y-}$ speciates in solution to give the di- and tri-protonated forms (Fig. 3) whereas $[H_mP_nW_{18}O_{62}]^{y-}$ can be observed as the hexa-, penta- and tetra-protonated forms (Fig. 4).

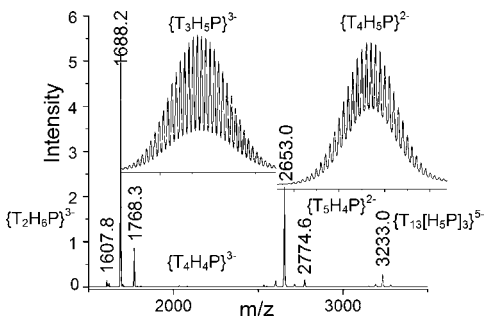

Fig. 4 The negative ion mass spectrum of $[H_mP_nW_{18}O_{62}]^{y-}$ showing the series of tetra-, penta- and hexa-protonated forms of $(TBA)_y[H_xP_1W_{18}O_{62}]^{(11-(x+y))-}$ in solution. T: TBA^+; P: $P_1W_{18}O_{62}$ (intensity × 10^4).

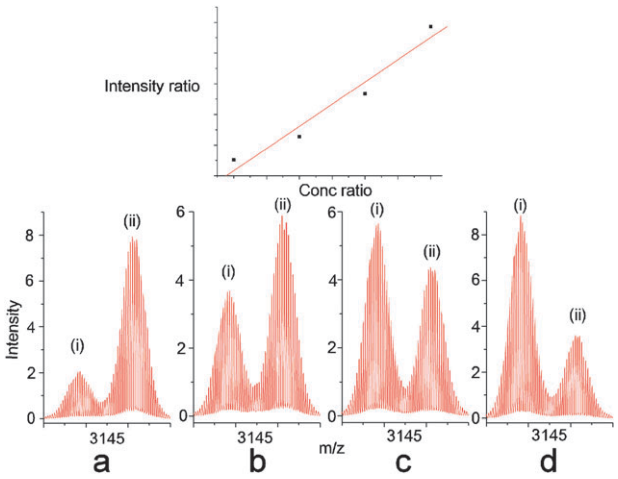

Fig. 5 Positive ion mass spectra (m/z range 3120 to 3170) of the $\{P_xW_{18}\}$ species (3138 m/z for $\{(TBA)_8[H_5PW_{18}O_{62}]\}^{2+}$) (i) and (3152 m/z $\{(TBA)_8[P_2W_{18}O_{62}]\}^{2+}$) (ii) recorded when varying the ratios of Solution A (0.007 mmol·$\mathbf{L}^{-1}$ $(TBA)_6[H_5PW_{18}O_{62}]$ in CH_3CN) and Solution B (0.028 mmol·$\mathbf{L}^{-1}$ $(TBA)_6[P_2W_{18}O_{62}]$ in CH_3CN). Spectrum a: 1 ml A + 1 ml B; Spectrum b: 2 ml A + 1 ml B; Spectrum c: 4 ml A + 1 ml B; Spectrum d: 6 ml A + 1 ml B.

This shows that heteropolyoxometalate clusters exist in solution in a range of accessible protonation states that can often not be identified by bulk analytical methods. For both compounds the most intense single ion signal or base peak was observed for the di- and penta-protonated species, respectively, and shows that it is possible to observe the protonation of a heteropoly acid as a function of the number of hetero-anions included within the cluster. Also, using this data, it is possible to assign the protonation state of the cluster in the solid state.

Furthermore, using a range of mixed-cluster ESI-MS experiments done as a function of concentration we were able to quantify the transmitted ion intensity directly with the concentration of the cluster-species in solution. This was done by comparison of the bis-phosphate Dawson cluster $(TBA)_6[P_2W_{18}O_{62}]$ with the mono-phosphate $(TBA)_6[H_5P_1W_{18}O_{62}]$. This gave a linear correlation between the relative ion intensity and the ratio of the concentration of the two compounds in solution, see Fig. 5. This means that in organic solvents it is possible to use ESI-MS studies to directly probe the solution equilibria.[45] This is an interesting result opening up a new field in the exploration of POM reaction mechanisms and exploration of the species present in solution under a given set of conditions.[9d]

3.2 Solution identification of functionalized POMs

The functionalization of POM clusers *via* covalent grafting of organic functions allows the properties of the cluster to be tuned and allows us to introduce other functionality. In our recent work an asymmetric, functionalized Mn-Anderson cluster was designed and synthesized, $(TBA)_3[MnMo_6O_{18}(C_4H_6O_3NO_2)(C_4H_6O_3NH_2)]$,[9e] utilizing ESI-MS during the screening process of the reaction mixtures and fine adjustment of the experimental conditions of this labile system. Subsequently, the system was set up for crystallization, and the crystalline precipitates were isolated from

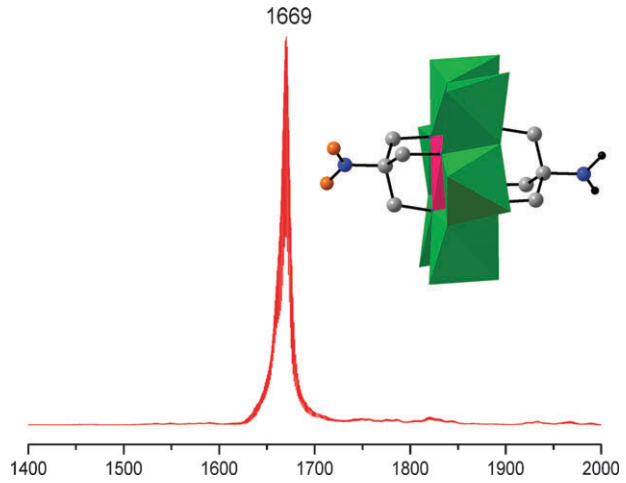

Fig. 6 ESI-MS spectrum of the asymmetric compound in MeCN shows one signal at m/z = 1669 due to $[(TBA)_2\{MnMo_6O_{18}(C_4H_6O_3NO_2)(C_4H_6O_3NH_2)\}]^-$ species. Inset: representation of the X-ray crystal structure of $\{MnMo_6O_{18}(C_4H_6O_3NO_2)(C_4H_6O_3NH_2)\}^{2-}$. Colour scheme – Mo: green polyhedra; Mn: pink polyhedron; C: grey; N: blue; O: orange; H: black.

the mother liquor by filtration every 6 hours. Each batch of the crystalline samples was then analysed again using electrospray ionization mass spectrometry (ESI-MS) in order to determine the distribution and number of products present, allowing the correct batch to be 'sorted' from the bulk, statistically defined mixture. The batch corresponding to the asymmetric compound was collected. Using this approach, ESI-MS studies not only helped the reaction mixtures to be 'sorted' but also allowed confirmation of the intrinsic composition, as shown in Fig. 6, and we were then able to go on to crystallize this product.

The peak at m/z = 1669 can be clearly assigned to the $[(TBA)_2\{MnMo_6O_{18}(C_4H_6O_3NO_2)(C_4H_6O_3NH_2)\}]^-$ anion. Additionally, the signal at m/z = 1669 is the only peak in the range of 1300 to 2000 m/z, with no peaks being observed that would be expected from the presence/contamination of the other possible species $[(TBA)_2\{MnMo_6O_{18}(C_4H_6O_3NH_2)_2\}]^-$ (1640 m/z) or $[(TBA)_2\{MnMo_6O_{18}(C_4H_6O_3NO_2)_2\}]^-$ (1700 m/z). The observation of such complex reaction mixtures under electrospray conditions is very important in an effort towards the design and synthesis of hybrid POM-based materials which possess desirable functionality.

3.3 Solution identification of new isopolyoxotungstates

In recent work, we targeted the exploration of aqueous solutions of isopolyoxotungstates using a combination of pH and anion control to unravel the influence of these factors on the self-assembly of anionic isopolyoxotungstates. As such we were able to demonstrate that it is possible to discover radically new cluster architectures in the isopolyoxotungstate family simply by acidifying solutions of sodium tungstate leading to the isolation and crystallization of an 'S'-shaped $[H_4W_{22}O_{74}]^{12-}$ cluster at pH 3.4 as $Na_{12}[H_4W_{22}O_{74}]\cdot 31H_2O$[8c] (Fig. 7).

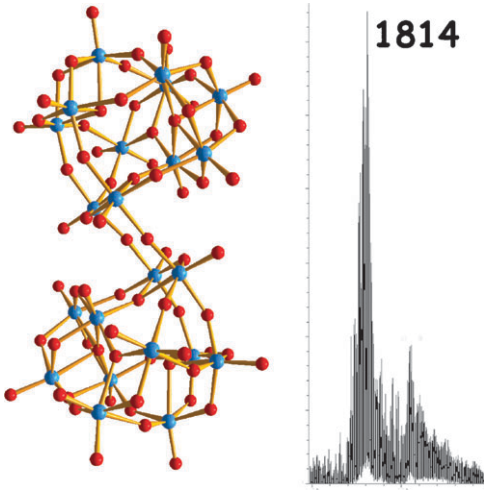

Fig. 7 The crystal structure of the 'S'-shaped cluster (left) and the negative ion mass spectrum for $\{(Na_9)[H_4W_{22}O_{74}]\}^{3-}$ in water (right). Simulation of the expected spectrum matches that of the observed peak at 1814 m/z.[8c] Colour scheme – W: blue; O: red.

The compound $Na_{12}[H_4W_{22}O_{74}]\cdot 31H_2O$ could not only be identified as containing the $[H_4W_{22}O_{74}]^{12-}$ anion in the solid state, but it was also identified in aqueous solution using ESI-MS analysis as the $\{(Na_9)[H_4W_{22}O_{74}]\}^{3-}$ anion at 1814 m/z. The cluster framework $[H_4W_{22}O_{74}]$ can unambiguously be assigned as being present, but the broad spectrum is simply due to the presence of several overlapping species arising from the many different envelopes. All these species are ions with a charge of 3– containing different amount of sodium ions and protons. On lowering the pH to 2.4, a related '§'-shaped $[H_{10}W_{34}O_{116}]^{18-}$ cluster is isolated as $Na_{18}[H_{10}W_{34}O_{116}]\cdot 47H_2O$ (Fig. 8).

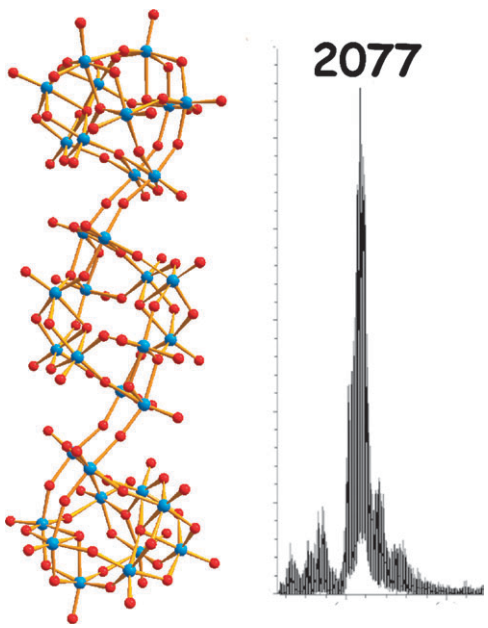

Fig. 8 The crystal structure of the '§'-shaped cluster (left) and the negative ion mass spectrum for $\{(Na_8)(H_6)[H_{10}W_{34}O_{116}]\}^{4-}$ in water (right). Simulation of the expected spectrum matches that of the observed peak at 2077 m/z.[8c] Colour scheme – W: blue; O: red.

$Na_{18}[H_{10}W_{34}O_{116}]\cdot 47H_2O$ contains the cluster as $[H_{10}W_{34}O_{116}]^{18-}$, but the cluster is identified in water as a $\{(Na_8)(H_6)[H_{10}W_{34}O_{116}]\}^{4-}$ species, as shown in Fig. 6 using mass spectrometry. Also, the cluster framework $[H_{10}W_{34}O_{116}]$ can unambiguously be assigned as being present but, once again, the broad spectrum is simply due to the presence of several overlapping species arising from the many different envelopes. In this case, all the species are ions with a charge of 4– containing different amounts of sodium ions and protons. The observation of such complex isopolytungstate-based clusters under electrospray conditions was not expected due to the number of possible species and the fragile nature of such clusters, but at the same time this opens up many new possibilities for the systematic screening of reactions to discover new cluster architectures.

3.4 Solution identification and isolation of mixed-metal/valence POMs with CSI-MS

ESI-MS studies have been extremely helpful in an effort to identify the composition, the extent of protonation, and the existence of other relatively stable species in the solution. However, these studies can be limited when we have to deal with labile clusters, with complex compositions, or those that adopt large and unstable motifs. Furthermore, given the extent of ionization and instability issues of such structures at high temperatures, it is often difficult to establish the presence of some cluster architectures using ESI-MS. This is because the fragmentation of labile POM clusters occurs at relatively high temperatures (150–200 °C) used to desolvate during the ESI process. In contrast, the low temperatures accessible (minimum −100 °C) for use with a cryospray source minimize uncontrolled fragmentation and so allow efficient transfer of very high nuclearity, yet labile, ionic species into the detector with minimal interfering effects from the ionization and desolvation processes.[35] By employing this approach, it is then possible to transfer many of the labile species present in solution into the mass spectrometer and so allow some correlation between the essentially gas phase measurements with solution and solid state studies.[26,35] At this point CSI-MS studies can offer the necessary environment for labile/unstable species to survive and collect important information towards understanding the self-assembly mechanisms in supramolecular chemistry.

3.5 Mixed-metal/valence hetero-POMs $V_2 \subset \{M_{17}V_1\}$

Recently, we reported our first attempts to detect and study labile POM systems using CSI-MS. CSI-MS studies proved to be a tool of vital importance in first identifying these species using the correct combination of experimental parameters to minimize fragmentation allowing observation of new cluster architectures in solution, and then providing some indication of how the synthetic procedure can be optimized to yield the new architecture.[26,50] In this work, we aimed to replace the heteroanion templates in the classical Dawson-like clusters *e.g.* $[W^{VI}{}_{18}O_{54}(PO_4)_2]^{6-}$ with transition metals; by scanning the reaction mixtures before crystallization we were able to locate the reaction systems that produced the $V_2 \subset \{M_{17}V_1\}$ species, as shown in Fig. 9.

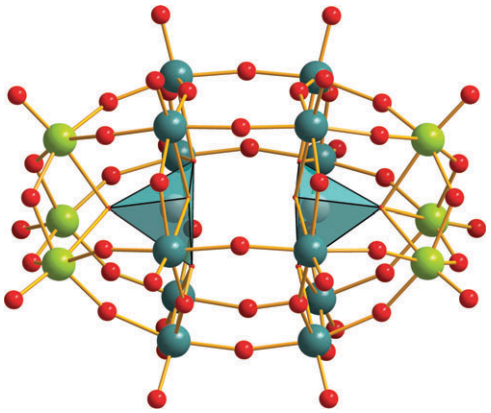

Fig. 9 Representation of the iso-structural anionic framework found in the structures of compounds with the general formula $[H_2V^{IV}M_{17}O_{54}(V^{V}O_4)_2]^{6-}$ (M = W or Mo). The $\{M_{17}V_1\}$ framework is shown in ball and stick and the V templates are shown by the polyhedra. Even though the 'framework' V^{IV} ion cannot be formally located, theoretical calculations showed a preference for the two cap positions rather than the belt positions. Colour scheme – Mo/W: blue; dark green (belt), light green (cap); O: red; V: dark green polyhedra.[26]

The discovery studies were performed by precipitating solids from a range of candidate reaction systems under aqueous conditions. The precipitates were then transferred into the organic phase by ion exchange with tetrabutylammonium (TBA) and 'screened' using CSI-MS. These studies showed that this family of clusters was present in solution prior to their structural analysis. The studies also showed that the TBA salts of the $\{M_{17}V_3\}$ clusters dissolve in acetonitrile (M = W, Mo) and that the clusters are stable in solution (Fig. 10). A range of charge (−1 to −3) and protonation (0–2) states were observed. Also the direct observation of $\{(TBA)_8[H_2V^{V}{}_2V^{IV}W_{17}O_{62}]\}^{2+}$ allows us to confirm that the clusters observed in the solid state all have six cations associated, and are di-protonated.

This observation is useful since this gives unambiguous proof that the Dawson capsules are present in solution, establishes the existence of a vanadium metal centre on the shell of the Dawson framework (which is almost impossible to distinguish crystallographically) and also confirms the extent

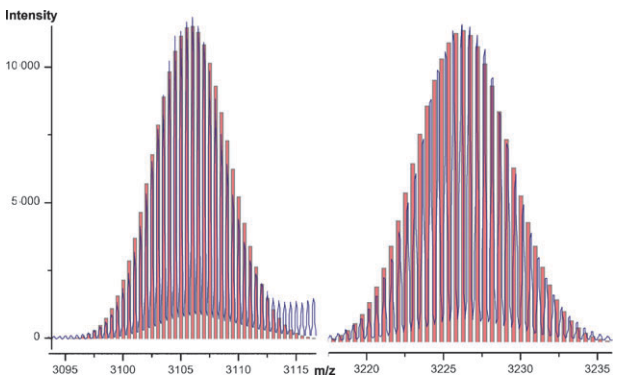

Fig. 10 Positive ion CSI mass spectrum showing the $\{(TBA)_{10-n}[H_nV^{V}{}_2V^{IV}W_{17}O_{62}]\}^{2+}$ in acetonitrile solution. Left: where $n = 2$ at m/z *ca.* 3106, right: where $n = 1$ m/z *ca.* 3227. The blue line shows the actual spectrum, and the red bar graph is the predicted envelope.

of protonation of the cluster, which is extremely difficult to determine directly.

Another challenging case is the mixed-metal/valence sulfite POM systems. The discovery of such species in solution, characterization and final optimization of the synthetic conditions proved to be an intriguing task. Recently, the diversity of vanadium-sulfite systems[51,52] in aqueous media has been investigated and a similar behaviour was found in this case as well. In this investigation, CSI-MS proved to be an important technique in our efforts to discover new Dawson-like capsules in solution, allowing the compound to be identified prior to structural analysis. CSI-MS studies of the TPA salts of the cluster (Fig. 11a) dissolved in acetonitrile confirmed that the sulfite capsule retained its integrity in solution, and peaks were seen that were assigned to $\{(TPA)_4[H_{1-n}V^{V}_{5+n}V^{IV}_{2-n}\ Mo_{11}O_{52}(SO_3)]\}^{2-}$ where $n = 1$ (with only one vanadium ion in oxidation state IV), giving an envelope centred at m/z *ca.* 1534.5, and where $n = 0$ (with two vanadium ions in oxidation state IV, requiring one proton), giving an envelope centred at m/z *ca.* 1535.0 (Fig. 11b).

It is possible to examine the aqueous reaction mixtures directly, but this often results in the observation of a plethora of species resulting from the multitude of possibilities arising from the clusters transferring into the MS detector with sodium and potassium cations with multiple water ligands. When using aqueous solutions, there can also be ion transfer problems resulting in very low intensity signals, which can be difficult to analyse in detail. Therefore, ion exchange and phase transfer to organic solvent enables the individual cluster species to be assigned directly.

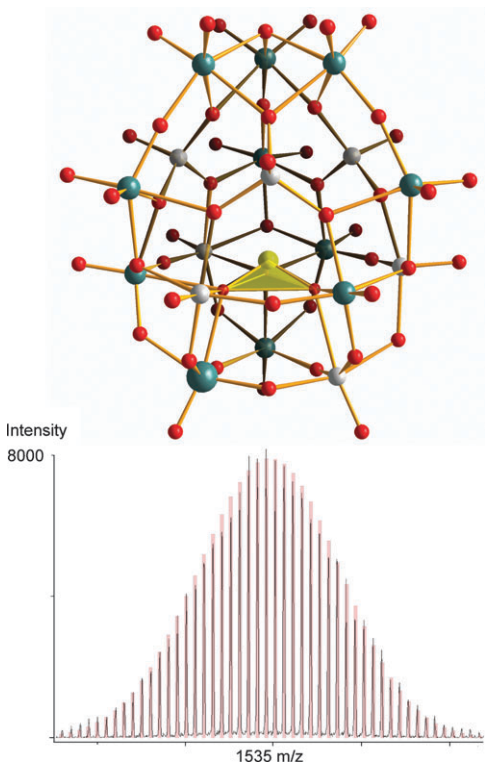

Fig. 11 (a) Ball-and-stick representation of the $[Mo^{VI}_{11}V^{V}_{5}V^{IV}_{2}O_{52}(\mu_9\text{-}SO_3)]^{7-}$ capsule anion. Colour scheme – Mo: green; O: red; V: grey; S: yellow polyhedron. (b) Negative ion mass spectrum in acetonitrile solution of $\{(TPA)_4[H_{1-n}V^{V}_{5+n}V^{IV}_{2-n}Mo_{11}O_{52}(SO_3)]\}^{2-}$. Black line: experimental data. Red bars: simulation of isotope pattern.

In the above examples, the application of CSI-MS to investigate and discover labile or unstable cluster species in solution was used to help discover and then optimize the synthetic approach to isolate the clusters and this proved to be of major significance. This is because when we carried out the same studies in ESI mode on the same series of solutions, we observed excessive fragmentation, which leads to a mixture of many different kinds of species revealing different compositions, oxidation states and possible structures. The combination of solution control (adjustment of solution in terms of pH, metal ion concentration, temperature and pressure) allows the direct observation of the species present in the reaction system with CSI-MS: an approach that we have recently found useful to observe reactive building blocks[53] and high nuclearity clusters.[7] In this context, we are utilizing CSI-MS in order to identify new POM clusters with novel templates and architectures that would not easily be isolated without prior detailed knowledge of the clusters present in the reaction solutions.

3.6 Periodate-containing POMs

In an extension of this technique to look at reactive clusters, we utilized CSI-MS studies in order to identify and unambiguously reveal the composition of a new cluster species in solution and investigate the relationship between solution and solid state. In this work, we explored the insertion of new, high oxidation state guests into the 'Dawson capsule' in order to allow modulation of the cluster's physical properties, *e.g.* redox and catalytic properties, and acidity. The encapsulation of such templates should significantly affect the acidic, catalytic, and redox properties of the resulting cluster systems. In this work, we examined the tungsten Dawson capsule, $K_6[H_3W_{18}O_{56}(IO_6)]\cdot 9H_2O$, which we have both synthesized and characterized in the solid state.[8d] To rule out the possibility that the aforementioned compound could be assigned as $[H_4W_{19}O_{62}]^{6-}$ (*i.e.* I substituted for W or other heteroions), we utilized high resolution CSI and ESI-MS to identify the exact elemental constitution of the cluster anion. To simplify the MS experiments, the potassium salt of the aforementioned compound was ion-exchanged with tetrapropylammonium cations (TPA^+), yielding $(TPA)_6[H_3W_{18}O_{56}(IO_6)]$. Fig. 12 shows the mass spectrum of $(TPA)_6[H_3W_{18}O_{56}(IO_6)]$ in acetonitrile in which all major peaks are related to $\{W_{18}I\}$ and can be assigned m/z 2588.1 $\{TPA_4[H_3IW_{18}O_{62}]\}^{2-}$, 2607.1 $\{TPA_4K[H_2IW_{18}O_{62}]\}^{2-}$ and 2680.7 $\{TPA_5[H_2IW_{18}O_{62}]\}^{2-}$.

In contrast, the TPA^+ salt of $[H_4W_{19}O_{62}]^{6-}$[9d] in acetonitrile gives a different mass spectrum in this m/z range: 1676.5 $\{TPA_3[H_2W_{19}O_{61}]\}^{3-}$, 1682.5 $\{TPA_3[H_4W_{19}O_{62}]\}^{3-}$, 1744.5 $\{TPA_4[H_3W_{19}O_{62}]\}^{3-}$, 2617.4 $\{TPA_4[H_4W_{19}O_{62}]\}^{2-}$, and 2709.9 $\{TPA_5[H_3W_{19}O_{62}]\}^{2-}$. Therefore, CSI mass spectral studies, in combination with elemental analysis and crystallography, have given us unambiguous proof of the existence and integrity of $\{W_{18}I\}$ species.

3.7 Probing the formation of POM-based nano-structures

The extension of MS studies to supramolecular architectures poses several important questions regarding the nature of the

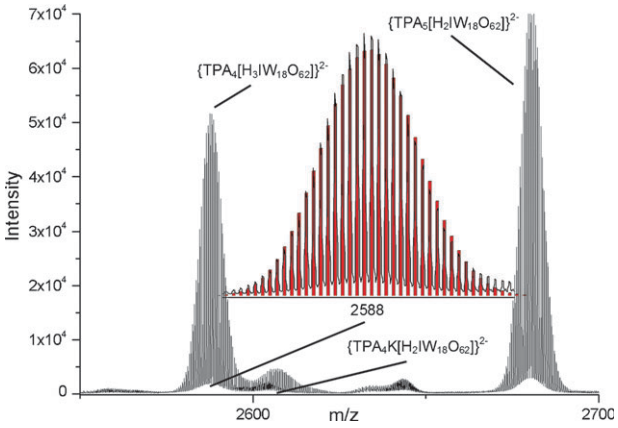

Fig. 12 Assigned negative-mode mass spectrum of $(TPA)_6[H_3IW_{18}O_{62}]$ in acetonitrile. An expansion of the peak at m/z = 2588 is shown along with the calculated isotopic pattern (red columns).

assemblies present in solution *vs.* those transmitted and observed in ESI-MS experiments. However, we have also made progress here as shown by the synthesis and characterization of a nano-structured POM-based assembly in the solid state.[54] By grafting of a H-bonding donor 'cap' onto a POM cluster, we can control the supramolecular self-assembly of cluster species in solution, as well as in the solid state, leading to the formation of macromolecular H-bonded nano-assemblies of polyoxometalate clusters. Most importantly, it was observed that the formation of these supramolecular architectures can be externally controlled by simply changing the grafted H-bonding organic cap (Fig. 13). In this case, CSI-MS studies did not only help us to identify and establish the integrity of the cluster but also to observe the formation of hydrogen-bonded nano-structures in the solution as well as to reveal information about the mechanism of this self-assembly process.

By using cryospray experiments at −40 °C we were able to examine the self-assembly processes in solution in great detail. For instance, cryospray mass spectrometric studies of $(TBA)_4H_2[H_2NC(CH_2O)_3P_2V_3W_{15}O_{59}]$ in dilute

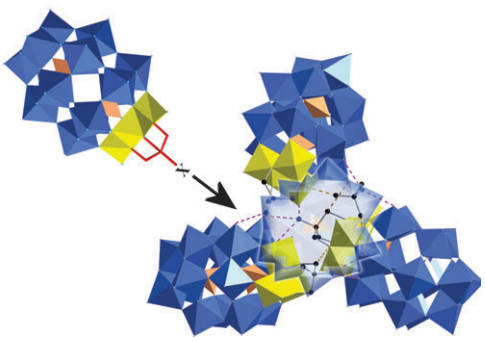

Fig. 13 Hydrogen-bonded distorted tetrahedral nano-assembly of $[H_2N\text{-}C(CH_2O)_3P_2V_3W_{15}O_{59}]^{6-}$ cluster. One lobe of the tetrahedron—pointing towards the observer—is made transparent for easy visualization of the H-bonding interactions. Colour scheme – O: cyan; W: blue; V: yellow; PO_4: peach polyhedra, where X = $–NH_2$, $–NO_2$ and $–CH_3$.

acetonitrile solutions revealed that the tris(hydroxymethyl)-aminomethane-grafted POM cluster exists in solution phase as monomers, dimers and trimers, and also the tetramer could be clearly observed. Peaks associated with the monomer species $\{(TBA)_4[H_2NC(CH_2O)_3P_2V_3W_{15}O_{59}]\}^{2-}$ and $\{(TBA)_5[H_2NC(CH_2O)_3P_2V_3\ W_{15}O_{59}]\}^{1-}$ can be found at m/z values 2502.2 and 5247.2, respectively, the dimer $\{(TBA)_9[H_2NC(CH_2O)_3)P_2V_3W_{15}O_{59}]_2\}^{3-}$ at m/z value 3416.7 and trimer $\{(TBA)_{14}[H_2NC(CH_2O)_3P_2V_3W_{15}O_{59}]_3\}^{4-}$ at m/z 3874.5. The observed mass and charge corresponding to each of these peaks clearly matched with the assigned formulae as well as the simulated spectra. Following observations in the mass spectra of the monomer, dimer and trimer, we were able to assign the peak at m/z 4149.5 to the tetrameric species $\{(TBA)_{19}[H_2NC(CH_2O)_3P_2V_3W_{15}O_{59}]_4\}^{5-}$.

The role of the H-bonding ability of the organic cap of the cluster anions in forming the multiple aggregation of cluster species in solution and gas phase was examined by comparing the cryospray mass spectra of cluster species $[H_2NC(CH_2O)_3P_2V_3W_{15}O_{59}]^{6-}$ (**1**), $[O_2NC(CH_2O)_3P_2V_3W_{15}\ O_{59}]^{6-}$ (**2**) and $[H_3CC(CH_2O)_3P_2V_3W_{15}O_{59}]^{6-}$ (**3**) under identical experimental conditions.

It was observed that the $–NO_2$ tipped cluster (**2**) also forms multiple aggregates in solution and gas phases, quite similar to cluster (**1**). Interestingly, it was found that the $–NO_2$ capped cluster is more efficient in forming such multiple aggregates in solution since assemblies of five (pentamer) and even six (hexamer) alkoxy POM clusters are observed in the case of cluster $[O_2NC(CH_2O)_3P_2V_3W_{15}\ O_{59}]^{6-}$. The weakly hydrogen-bonding $–CH_3$ tipped cluster forms mainly monomeric species in solution, and no higher aggregates are observed (Fig. 14). The aforementioned CSI-MS studies presented an approach to observe the formation of nano-assemblies of polyoxometalate clusters in solution and in the gas phase. Moreover, these studies have given us important missing information on the 'mechanism' that governs this assembly process. The strategy to attach an organic fragment to a polyoxometalate to direct its supramolecular assembly resulting in ultra-large hydrogen-bonded nano-architectures that can be observed in solution, as well as the solid state, has been achieved.

The observation of the gigantic hydrogen-bonded tetrahedral nano-assembly of the alkoxy cluster anions of $[H_2NC(CH_2O)_3P_2V_3W_{15}O_{59}]^{6-}$ along with 19 TBA counterions in solution phase by CSI-MS analysis underlines the potential of this technique to investigate the role of weak interactions such as hydrogen-bonding in understanding the self-organization processes involved in the synthesis of novel POM-based functional nanomaterials.

3.8 Mechanistic insights into POM self-assembly

Given the power of CSI-MS to look in detail at labile POM solutions, we envisaged utilizing this technique in order to shed light upon the mechanism of self-organization of an individual POM molecule from its reagents in solution.

The study of the self-assembly processes of POMs has previously been pursued by the use of ligands with well-defined binding sites. This allows easier elucidation of the assembly processes as the POM units effectively behave like

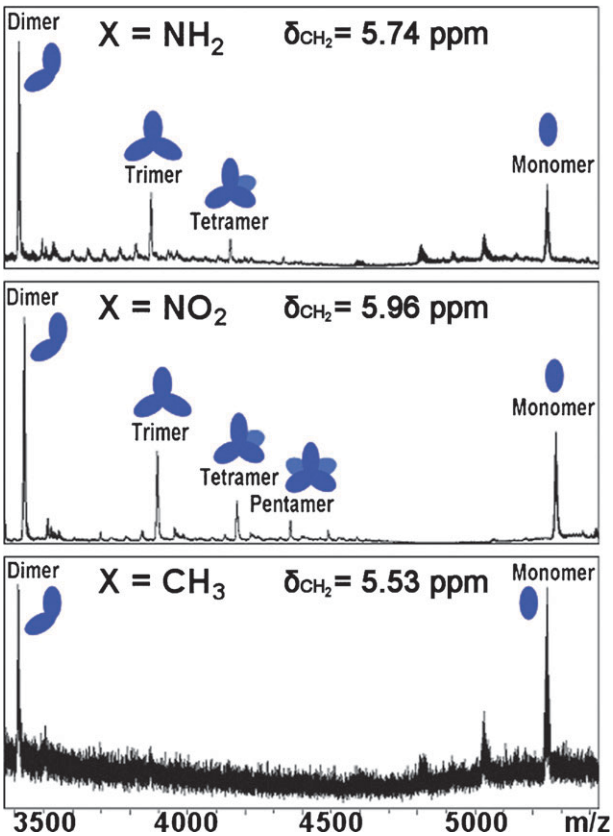

Fig. 14 Comparison of the CSI-MS spectra and supramolecular assemblies of clusters **1** ($-NH_2$), **2** ($-NO_2$) and **3** ($-CH_3$) as a function of different substituent (X) on the organic cap. Spectra are on the same m/z scale.

multi-dentate organic ligands and bind readily to secondary transition metals.[55] It was for these reasons that the use of silver(I) cations as linking groups between POM units has been investigated within the Cronin group. It was found that in the reaction of $[TBA_2(Mo_6O_{19})]$ with silver(I) fluoride in a mixed acetonitrile–methanol solution, a unique one-dimensional chain structure of the composition $(TBA_{2n}[Ag_2Mo_8O_{26}]_n)$ is produced. Furthermore, many other architectures, involving specifically the aggregation of $\{Ag(Mo_8)Ag\}$ synthons, have been produced.[56] The generation of these different POM architectures has been shown as governed mainly by the steric requirements of the organic cations or coordinated solvent molecules. See Fig. 15 below for a structural representation of the $\{Ag(Mo_8)Ag\}$ synthon.

In this work, the in-solution inter-conversion of Lindqvist into β-octamolybdate anions and subsequent self-assembly into the silver-linked POM structure $[(n\text{-}(C_4H_9)_4N)_{2n}(Ag_2Mo_8O_{26})_n]$ was investigated using CSI-MS and electronic absorbance spectroscopy.[57] The application of CSI-MS, in conjunction with electronic absorbance spectroscopy, allowed the direct monitoring of real-time re-arrangements in a POM reactant solution. Further, the combination of these approaches allowed us to directly observe the re-arrangement of Lindqvist anions into the $\{Ag(Mo_8)Ag\}$ synthon units and the subsequent wrapping of the one-dimensional silver-octamolybdate synthons with organic cations.

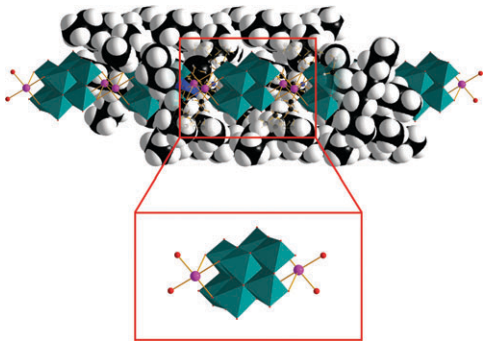

Fig. 15 Structural representation of the silver-linked β-octamolybdate chain wrapped in 'encapsulating' TBA^+ cations which makes up the structure of $((n\text{-}C_4H_9)_4N)_{2n}(Ag_2Mo_8O_{26})_n$. The organic cations are partially removed to reveal the encapsulated chain structure (top). The $\{Ag(Mo_8)Ag\}$ synthon unit, the building block of this chain, is highlighted below. Colour scheme: Mo: green polyhedra; Ag: pink; O: red; N: blue; C: black; H: white.

Only mono-anionic and di-anionic series were observed in these results, from approximately 285 m/z to as high as approximately 3800 m/z, indicating the efficient transfer of very high nuclearity, yet labile, ionic species into the detector with minimal interfering effects from the ionization and desolvation processes. The six mono-anionic series identified within these results were:

(i) $[Mo_mO_{3m}]^-$ where m = 2, 3 or 5
(ii) $[HMo_mO_{3m+1}]^-$ where m = 2 to 6
(iii) $[H_7Mo_mO_{3m+2}]^-$ where m = 2 to 6
(iv) $[H_7Mo_mO_{3m+3}]^-$ where m = 2 to 5
(v) $[H_9Mo_mO_{3m+4}]^-$ where m = 2 to 6
(vi) $[AgMo_mO_{3m+1}]^-$ where m = 2 to 4

From these identified anion series (see Fig. 16), only series (ii) has been observed in previous ESI-MS studies on polyoxomolybdate systems,[29] which underpins the advance in understanding that can be made with CSI-MS studies for detecting molecular building blocks. Anion series (vi) is of special interest with regard to this POM reaction system. This is because the role of the Ag^I moiety in the assembly of the stable silver-linked octamolybdate species has been observed

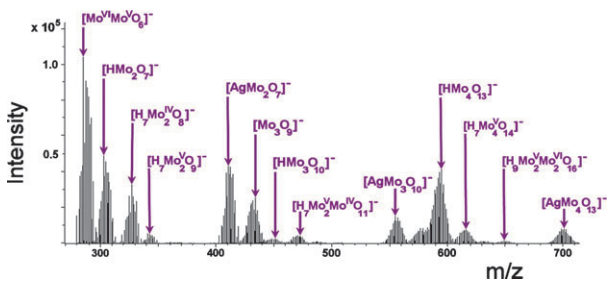

Fig. 16 CSI-MS data collected for the reaction solution. The six mono-anionic series identified within these results are highlighted. The steps towards the assembly of the $\{Ag(Mo_8)Ag\}$ synthon units can be observed by examination of anion series (vi) which highlights the role of the Ag^+ in the re-arrangement process of these clusters. Of particular note from this series are the peaks at 410.7 m/z and 700.5 m/z which are attributed to the species $[AgMo_2O_7]^-$ and $[AgMo_4O_{13}]^-$, respectively.

by mass spectral methods for the first time and is shown to be crucial for the formation of the larger cluster fragments.

Detection of the $[AgMo_2O_7]^-$ fragment (peak at 410 m/z) of the (Ag{Mo_8}Ag) synthon from the reaction solution supports the theory of re-arrangement of the Lindqvist anion into $[AgMo_2O_7]^-_n$, which is the smallest stable unit of the silver-linked POM chain. Indeed the stable nature of this fragment of the (Ag{Mo_8}Ag) synthon unit allowed the isolation in the solid state of $Ag_2Mo_2O_7$ clusters linked into a chain formation by Gatehouse and Leverett.[58] Detection of the $[AgMo_4O_{13}]^-$ species (peak at 700.5 m/z), being half the (Ag{Mo_8}Ag) synthon unit, represents the next stepping stone in the final re-arrangement to the stable silver-linked octamolybdate species (Fig. 17).

In the higher mass range of the CSI-MS analyses carried out, the structure-directing effect of the organic cations, hypothesized by our group in previous work, has been illustrated for the first time. Detection of the following species $[(AgMo_8O_{26})TBA_2]^-$ (peak at 1776.6 m/z), $[(Ag_2Mo_8O_{26})(Mo_4O_{13})TBA_3]^-$ (peak at 2718.3 m/z), and $[(Ag_2Mo_8O_{26})(Mo_8O_{26})TBA_5]^-$ (peak at 3796.5 m/z), each with an increasing organic cation contribution, shows the increasing metal nuclearity of the chain of polymer compound concomitant with the associated increase in organic cations present (Fig. 18). This observation can be interpreted as the start of the self-assembly aggregation process where 'monomeric' units assemble into larger fragments, which eventually leads to the formation of crystals of compound $(TBA_{2n}[Ag_2Mo_8O_{26}]_n)$.

To investigate the kinetics of the rearrangement process of Lindqvist anions into (Ag{Mo_8}Ag) synthons in the reaction solution, electronic absorbance studies were used to monitor the decrease of the Lindqvist anion absorption band at λ = 355 nm over time.[59] The relationship between decreasing Lindqvist anion concentration and concomitant increase in {Mo_8} anion concentration was further supported by monitoring the reaction solution over time using CSI-MS experiments. It can be seen from these results (see Fig. 19)

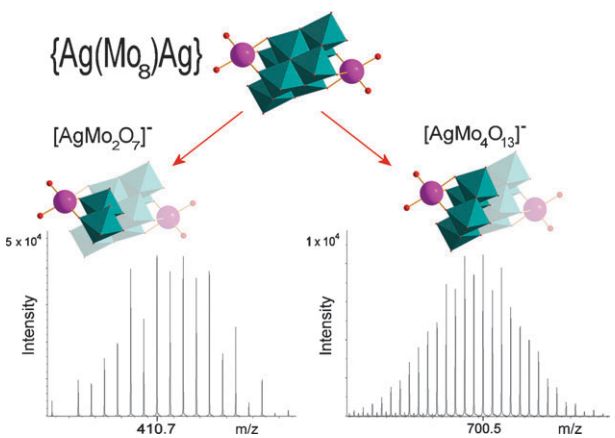

Fig. 17 Representation of the $[AgMo_2O_7]^-$ and $[AgMo_4O_{13}]^-$ species identified within the CSI-MS analyses of the reaction solution. Top: representation of the $[AgMo_2O_7]^-$ and $[AgMo_4O_{13}]^-$ species as building blocks of the {Ag(Mo_8)Ag} synthon. Bottom: mass spectra of the isotopic envelopes for their corresponding mass peaks at 410.7 m/z and 700.5 m/z, respectively. Colour scheme – Mo: green polyhedra; Ag: pink; O: red.

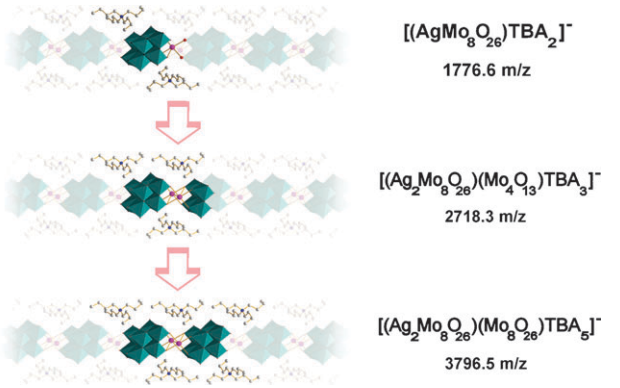

Fig. 18 Structural representation of the higher mass fragments (highlighted) identified within the CSI-MS analyses of a reaction solution. This diagram illustrates the increasing metal nuclearity of the chain concomitant with the associated increase in organic cations present. Colour scheme: Mo: green polyhedra; Ag: pink; O: red; C: grey; N: blue.

that the peak intensity of the reagent $[TBA(Mo_6O_{19})]^-$ decreases as the peak intensities recorded for the product species $[(AgMo_8O_{26})TBA_2]^-$ and $[(Ag_2Mo_8O_{26})TBA]^-$ increase. Interestingly, it can also be observed from these CSI-MS results that the recorded peak intensity of species $[AgMo_4O_{13}]^-$ (peak at 700.5 m/z) over reaction time appears to remain almost constant throughout. This may indicate an equilibrium state of $[AgMo_4O_{13}]^-$ concentration where the rearrangement of Lindqvist anions forms $[AgMo_4O_{13}]^-$ species, but these then continue rearranging into the larger reactive (Ag{Mo_8}Ag) building blocks.

In summary, the use of CSI-MS in this way to monitor real-time, in-solution rearrangements in a POM reactant solution is, to our knowledge, unprecedented. This approach can now be extended to investigate the bottom-up, in-solution processes governing the formation of other POM systems, so

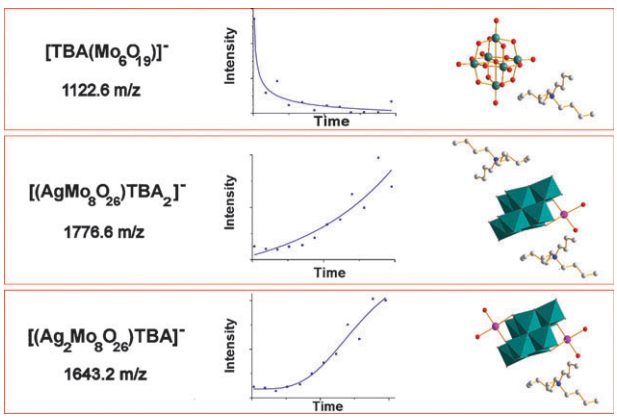

Fig. 19 Graphs showing peak intensities plotted against the time of CSI-MS data acquisition during the reaction of $TBA_2[Mo_6O_{19}]$ + AgF (best fits shown). The peak identities and m/z values of the peaks studied are shown (left) along with representations of the predicted structures of these species (right). Top: $[TBA(Mo_6O_{19})]^-$ at 1122.6 m/z. Centre: $[(AgMo_8O_{26})TBA_2]^-$ at 1776.6 m/z. Bottom: $[(Ag_2Mo_8O_{26})TBA]^-$ at 1643.2 m/z. Colour scheme – Mo, green polyhedra; Ag, pink; O, red; C, grey; N, blue.

enhancing our understanding and giving us the potential to control the building-block principles involved.

4. Species identification and probing structural transformations in multi-metallic systems

The diversity and effectiveness of CSI-MS studies has also been proven in the case of multi-metallic coordination systems. Careful scanning of $\{Co_{(12-x)}Ni_x\}$–tach (where tach: *cis*,*trans*-1,3,5-triaminocyclohexane) reaction mixtures of different concentration ratios allowed us to isolate the correct reaction conditions that lead to the identification, characterization and finally the formation of pure desirable products.[7a] The existence of a combinatorial library of Co–Ni species makes the system extremely difficult to characterize yet allows us to design multi-nuclear bimetallic magnetic materials.

Close examination of the ESI-MS data of the identified compounds clearly shows envelopes corresponding to the $\{Ni_{12}\}$ and $\{Co_{12}\}$ intact cluster species, which can each be assigned as $[Ni_{12}(CH_3O)_{12}(CH_3CO_2)_9(CO_3)(tach)_6]^+$ and $[Co_{12}(OH)_{12}(CH_3CO_2)_{10}(CO_3)(H_2O)_6(tach)_6(H)]^+$ (Fig. 20). Furthermore, the $\{Co_6Ni_6\}$ species gives a CSI-MS envelope which matches that expected for a discrete mixed species (containing $(OH)_6$ and $(CH_3O)_6$ groups), rather than the supposition of many possible outcomes (Fig. 20).

Moreover, we found that isostructural mixed Ni–Co clusters can be accessed by controlling the pH–metal ion ratio of the reaction solution after studying the system by CSI-MS, and these mixed systems can be observed using MS and isolated in the pH range of 3.5–10.5 (Fig. 21) as a function of pH and concentration ratios.

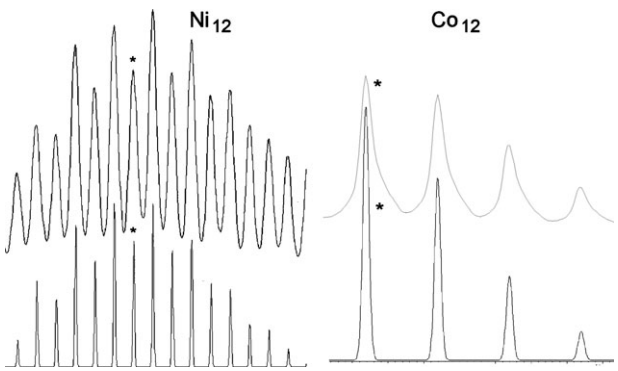

Fig. 20 Cryospray mass spectrum for the $\{M_{12}\}$ clusters at −40 °C. Experimental (top) and simulated data (below). Right: $[Co_{12}(OH)_{12}$–$(CH_3CO_2)_{10}(CO_3)(H_2O)_6(tach)_6H]^+$; * = 2445 *m*/*z*. Left: $Ni_{12}(CH_3O)_{12}$–$(CH_3CO_2)_9(CO_3)(tach)_6]^+$; * = 2442 *m*/*z* (simulated and experimental within 1 Da).

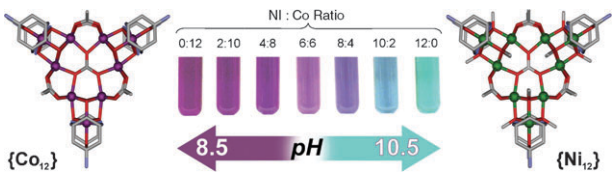

Fig. 21 Structures of the $\{Co_{12}\}$ and $\{Ni_{12}\}$ complexes and a schematic showing the colours of mixed $\{Ni_{12-n}Co_n\}$ (n = 1, 2. . ., 11) intermediates. Ni: green, Co: purple, C: grey, N: blue, O: red.

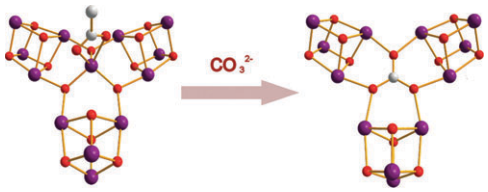

Fig. 22 Comparison of cores of $\{Co_{13}\}$ (left) and $\{Co_{12}\}$ (right), capping *trans*-tach ligands omitted for clarity.

Using the same conditions and solution identification technique we then isolated the $\{Co_{13}\}$ species, (Fig. 22, left) which represents the same structural motif with the aforementioned $\{M_{12}\}$ compounds and consists of three Co-cubanes that are bridged together through a $[CoO_3(OAc)]^{5-}$ unit. Utilizing CSI-MS studies we managed to observe the real-time structural transformation in solution of $\{Co_{13}\}$ to $\{Co_{12}\}$ daughter product by exchanging the central templating core $[CoO_3(OAc)]^{5-}$ for the carbonate anion (Fig. 22).[7b]

The above-mentioned observation also demonstrates that the $\{Co_{12}\}$ cluster core in solution originates from the $\{Co_{13}\}$ cluster core that forms in the absence of 'external' ligand templates, giving us important hidden information about what takes place during the self-assembly process. The ability to induce systematic transformations to a given molecular framework or supramolecular architecture, *i.e.* to fine-tune electronic or magnetic properties, is crucial in the design of functional molecule-based materials.

In another piece of work,[60] the use of CSI-MS studies has allowed the identification of a multi-metallic Cr-based species in solution formed by reactive $\{Cr_6\}$ species (Fig. 23), where the $\{Cr_6\}$ forms a larger complex *via* sodium fluoride interactions to give $[(NH_2Et_2)\{CrNa_{14}F_6(H_2O)_{10}\}\{Cr_6F_{11}(O_2CBu)_{10}\}_4]$.

Although ESI-MS measurements did not allow the observation of the intact cluster, CSI-MS experiments on a $\{Cr_{25}\}$ (Fig. 25) compound in THF–CH_3CN (70 : 30) at −40 °C showed that the supramolecular assembly is present as a di-cation (Fig. 24).

The parent cluster ion can be found in two overlapping envelopes centred at an *m*/*z* of *ca.* 3410.2. Two species can be identified that are related to the parent cluster. Both species

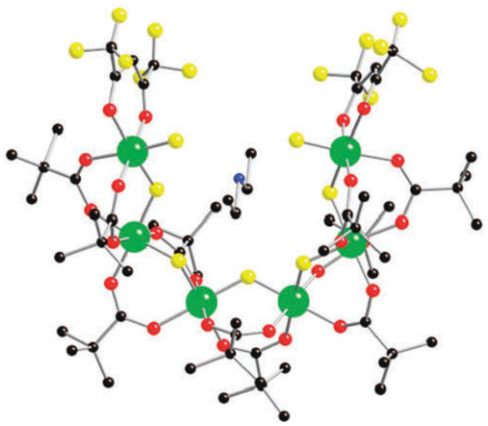

Fig. 23 The structure of $[(Et_2NH_2)\{Cr_6F_7(O_2CtBu)_{10}(hfac)_2\}]$ where hfac = 1,1,1,5,5,5-hexafluoroacetylacetonate. Colours: Cr: green; O: red; F: yellow; N: blue; C: black; Na: purple; H: not shown.

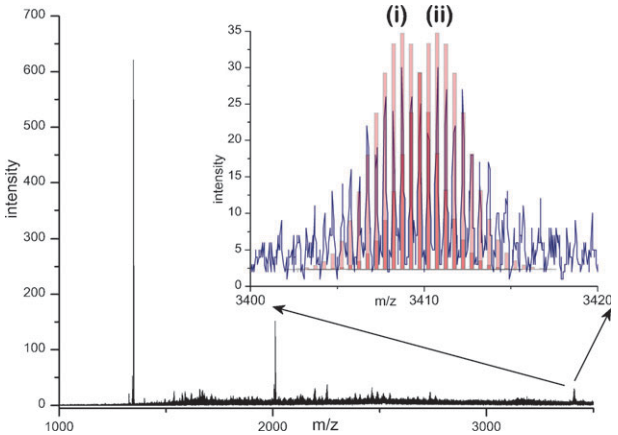

Fig. 24 CSI-MS of $[(NH_2Et_2)\{CrNa_{14}F_6(H_2O)_{10}\}\{Cr_6F_{11}(O_2CBu)_{10}\}_4]$ at 40 °C in THF–CH_3CN (70 : 30). The inset shows the molecular ion between 3400 and 3420 *m*/*z*. Two species can be clearly identified as being related to the parent cluster (blue spectrum); isotropic distributions calculated for species discussed in the text are shown by the faded red columns.

are doubly charged and the observed pattern corresponds to (i) $C_{204}H_{390}NCr_{25}F_{48}Na_{14}O_{89}$, (*i.e.* the molecular species – H_2O, – 2F: actual (3408.7 *m*/*z*), observed (3408.5 *m*/*z*)); and (ii) $C_{204}H_{388}NCr_{25}F_{50}Na_{14}O_{87}$ (*i.e.* the molecular species – H_2O, –2OH: actual (3410.8 *m*/*z*), observed (3410.5 *m*/*z*)) (Fig. 25).

The most unusual aspect of the aforementioned material is that the $\{Cr_6\}$ 'horseshoe' acts as a polynucleating fluoride donor and that the resulting supramolecular assembly has significant solution stability. CSI-MS is possibly the only tool currently available that can unambigously demonstrate the structural integrity of this complex in solution.

CSI-MS can also be used to observe intact multi-metallic coordination complexes in solution, and this has been illustrated through the work investigating a novel pentanuclear palladium(II) complex.[61] For example, we have designed ligand $\mathbf{L_1}$ (see Fig. 26) to interact with anionic species, and to coordinate to metal ions (e.g. possibly as a metallointercalator); however, ligand $\mathbf{L_1}$ is transformed to $\mathbf{L_2}$ upon complexation.[61]

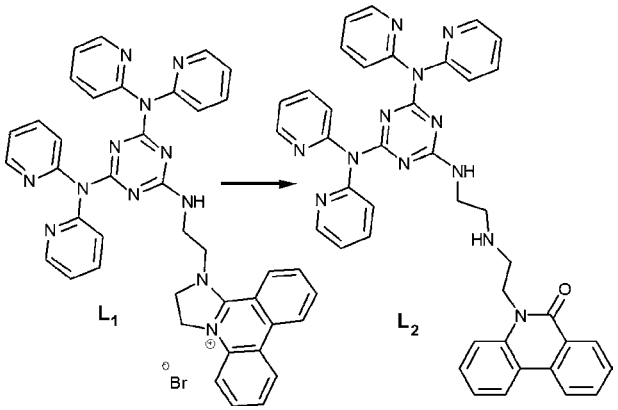

Fig. 26 The transformation of ligand $\mathbf{L_1}$ into $\mathbf{L_2}$ upon complexation with $Pd(OAc)_2$ in DCM *via* a ring-opening process; this occurs in a 33% yield.

On reaction of compound $\mathbf{L_1}$ with palladium(II) acetate in DCM, a pentanuclear Pd(II) complex is formed (Fig. 27) in which the Pd(II) mediates a ligand transformation of the aforementioned compound into a phenanthridone-based ligand ($\mathbf{L_2}$), see Fig. 26. The Pd(II) coordination compound has been characterized in the solid state *via* single-crystal X-ray crystallography and has been formulated as $[Pd_5(\mathbf{L_2})_2(OAc)_8](Br)_2$, see Fig. 27. CSI-MS investigations have also shown that the $Pd_5\mathbf{L_2}$ core can be observed in the solution state by the identification of the $[Pd_5(C_{40}H_{34}N_{12}O)_2(CH_3CO_2)_5Cl_6]^-$ anion at –40 °C, see Fig. 28.

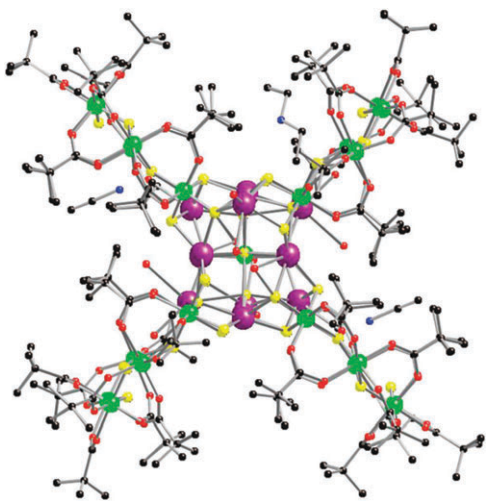

Fig. 25 Crystal structure of $[(NH_2Et_2)\{CrNa_{14}F_6(H_2O)_{10}\}\{Cr_6F_{11}(O_2CBu)_{10}\}_4]$ Colours – Cr: green; O: red; F: yellow; N: blue; C: black; Na: purple; H: not shown.

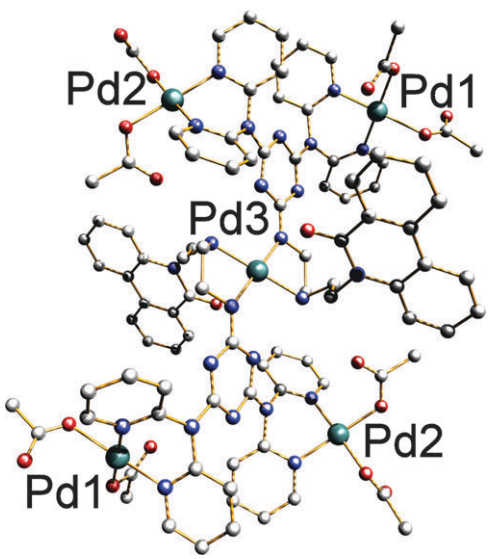

Fig. 27 Ball-and-stick representation of $[Pd_5(\mathbf{L_2})_2(OAc)_8]^{2+}$. The solvent and anions of crystallization, as well as the H atoms, are omitted for clarity. Colour scheme – C, grey; N, blue; O, red; Pd, green. Pd3 rests on an inversion centre.

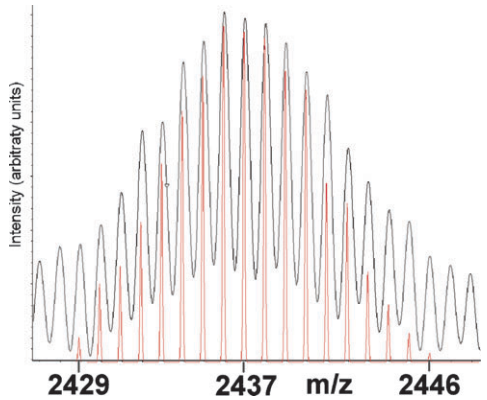

Fig. 28 Cryospray mass spectrum (negative ion mode) of $[Pd_5(\mathbf{L_2})_2(OAc)_8](Br)_2$ in a DCM–MeCN (1 : 1) mixture at −40 °C is shown in black. The observed anion is $[Pd_5(C_{40}H_{34}N_{12}O)_2(CH_3CO_2)_5Cl_6]^-$ and the simulated spectrum is shown in red.

Conclusions

In recent years, there has been an unprecedented rise in both the number of interesting supramolecular clusters that have been structurally characterized by single-crystal X-ray crystallography, and in the absolute size of the molecules characterized. Polyoxometalates and multi-metallic coordination compounds are ideal candidates for the development of a new type of supramolecular chemistry based upon the building-block ideas already established; using these ideas it should be possible to work towards designing nanomolecules of ever increasing size and complexity.

Utilizing the power of high resolution ESI and CSI-MS to investigate very large, labile frameworks will allow further exploration and expansion of our understanding of the building block principles that govern the bottom-up, self-assembly processes of inorganic complexes, supramolecular architectures, and cluster formation in solution. Furthermore, the extension of the use of ESI-MS and CSI-MS for identification of intermediate reactive species in many different (including catalytic) reaction mechanisms could yield an unprecedented level of detail allowing the determination of the reactive species as well as kinetic and parameters to be determined (subject to several limiting constraints being addressed) using variable temperature electrospray mass spectrometry. This is an important area for research as our increasing knowledge of these formation mechanisms will allow future design and directed synthesis of new POM and multi-metallic coordination clusters that adopt specific architectures and so possess particular functionality. The discoveries that have been discussed in this article clearly show that the first significant steps towards this goal have been accomplished.

In conclusion, the quest for the *a priori* controlled and directed self-assembly of complex functional molecules and materials is brought one step forward using these techniques and we may even be able to directly use mass spectrometry to guide synthetic routes to isolate desired products *via* real-time mass spectral screening of various reaction solutions, bridging the gap between self-assembly using serendipity and design. These techniques and approaches should have wide applicability across inorganic chemistry and supramolecular systems. It is now with excitement that one can consider the future implications of applying this approach to structure design and discovery across the broad field of organometallic, coordination and polyoxometalate chemistry and we will soon attempt to establish the feasibility of the new field of variable temperature electrospray mass spectrometry (VT-ESI-MS).

Acknowledgements

We would like to thank WestCHEM and the University of Glasgow for supporting this work with funds to purchase the equipment, and the Leverhulme Trust, Royal Society (London), and the EPSRC for funding this research. We would like to thank Bruker Daltonics for collaboration, advice, and the support of this work.

Notes and references

1 J. W. Steed and J. L. Atwood, *Supramolecular Chemistry*, John Wiley & Sons Ltd., Chichester, 2000.
2 C. Sanchez, G. J. de Soler-Illia, F. Ribot, T. Lalot, C. R. Mayer and V. Cabuil, *Chem. Mater.*, 2001, **13**, 3061.
3 D.-L. Long, P. Kögerler, L. J. Farrugia and L. Cronin, *Angew. Chem., Int. Ed.*, 2003, **42**, 4180.
4 L. Cronin, *Angew. Chem., Int. Ed.*, 2006, **45**, 3576.
5 L. Cronin, P. Kögerler and A. Müller, *J. Solid State Chem.*, 2000, **152**, 57.
6 R. E. P. Winpenny, *J. Chem. Soc., Dalton Trans.*, 2002, 1.
7 (*a*) G. J. T. Cooper, G. N. Newton, P. Kögerler, D.-L. Long, L. Engelhardt, M. Luban and L. Cronin, *Angew. Chem., Int. Ed.*, 2007, **46**, 1340; (*b*) G. N. Newton, G. J. T. Cooper, P. Kögerler, D.-L. Long and L. Cronin, *J. Am. Chem. Soc.*, 2008, **130**, 790.
8 (*a*) D.-L. Long, H. Abbas, P. Kögerler and L. Cronin, *J. Am. Chem. Soc.*, 2004, **126**, 13880; (*b*) D.-L. Long and L. Cronin, *Chem.–Eur. J.*, 2006, **12**, 3699; (*c*) H. N. Miras, J. Yan, D.-L. Long and L. Cronin, *Angew. Chem., Int. Ed.*, 2008, **47**, 8420; (*d*) D.-L. Long, Y.-F. Song, E. F. Wilson, P. Kögerler, S.-X. Guo, A. M. Bond, J. S. J. Hargreaves and L. Cronin, *Angew. Chem., Int. Ed.*, 2008, **47**, 4384.
9 (*a*) C. Ritchie, A. Ferguson, H. Nojiri, H. N. Miras, Y.-F. Song, D.-L. Long, E. Burkholder, M. Murrie, P. Kögerler, E. K. Brechin and L. Cronin, *Angew. Chem., Int. Ed.*, 2008, **47**, 5609; (*b*) C. Ritchie, C. Streb, J. Thiel, S. G. Mitchell, H. N. Miras, D.-L. Long, T. Boyd, R. D. Peacock, T. McGlone and L. Cronin, *Angew. Chem., Int. Ed.*, 2008, **47**, 6881; (*c*) D.-L. Long, C. Streb, Y.-F. Song, S. Mitchell and L. Cronin, *J. Am. Chem. Soc.*, 2008, **130**, 1830; (*d*) D.-L. Long, P. Kögerler, A. D. C. Parenty, J. Fielden and L. Cronin, *Angew. Chem., Int. Ed.*, 2006, **45**, 4798; (*e*) Y.-F. Song, D.-L. Long, S. E. Kelly and L. Cronin, *Inorg. Chem.*, 2008, **47**, 9137.
10 (*a*) G. Seeber, P. Kögerler, B. M. Kariuki and L. Cronin, *Chem. Commun.*, 2004, 1580; (*b*) G. Seeber, B. M. Kariuki and L. Cronin, *Chem. Commun.*, 2002, 2912.
11 (*a*) M. T. Pope, *Heteropoly and Isopoly Oxometalates*, Springer-Verlag, Berlin, 1983; (*b*) M. T. Pope and A. Müller, *Angew. Chem., Int. Ed. Engl.*, 1991, **30**, 34; (*c*) *Polyoxometalates: From Platonic Solids to Anti-Retroviral Activity*, ed. M. T. Pope and A. Müller, Kluwer Academic Publishers, Dordrecht, 1994; (*d*) *Polyoxometalate Chemistry From Topology* via *Self-Assembly to Applications*, ed. M. T. Pope and A. Müller, Kluwer Academic Publishers, Dordrecht, 2001; (*e*) *Polyoxometalate Chemistry for Nano-Composite Design*, ed. T. Yamase and M. T. Pope, Kluwer Academic/Plenum Publishers, New York, 2002.
12 (*a*) *Polyoxometalate Molecular Science NATO Science Series II*, ed. J. J. Borras-Almenar, E. Coronado, A. Müller and M. T. Pope, Kluwer Academic Publishers, Dordrecht, 2003, vol. 98; (*b*) M. T. Pope, Polyoxo Anions: Synthesis and Structure, in *Comprehensive Coordination Chemistry II: Transition Metal Groups 3–6*, ed. A. G. Wedd, Elsevier Science, New York, 2004, vol. 4,

pp. 635–678; (*c*) C. L. Hill, Polyoxometalates: Reactivity, in *Comprehensive Coordination Chemistry II: From Biology to Nanotechnology*, ed. A. G. Wedd, Elsevier, Ltd., Oxford, UK, 2004, vol. 4, pp. 679–759; (*d*) L. Cronin, in *Comprehensive Coordination Chemistry II*, ed. J. A. McLeverty and T. J. Meyer, Pergamon, Oxford, 2004, ch. 7.3, vol. 7, pp. 1–57.

13 (*a*) R. E. P. Winpenny, in *Comprehensive Coordination Chemistry II*, ed. J. A. McCleverty and T. J. Meyers, Pergamon, Oxford, 2004, ch. 7.3, vol. 7, pp. 125–175; (*b*) R. E. P. Winpenny, *Chem. Soc. Rev.*, 1998, **27**, 447; (*c*) M. Murugesu, W. Wernsdorfer, K. Abboud and G. Christou, *Angew. Chem., Int. Ed.*, 2005, **44**, 892.

14 (*a*) D. Gatteschi and R. Sessoli, *Angew. Chem., Int. Ed.*, 2003, **42**, 268; (*b*) E. K. Brechin, E. C. Sanudo, W. Wernsdorfer, C. Boskovic, J. Yoo, D. N. Hendrickson, A. Yamaguchi, H. Ishimoto, T. E. Concolino, A. L. Rheingold and G. Christou, *Inorg. Chem.*, 2005, **44**, 502; (*c*) A. Tasiopoulos, A. Vinslava, W. Wernsdorfer, K. Abboud and G. Christou, *Angew. Chem., Int. Ed.*, 2004, **43**, 2117.

15 First report of structure of $[Mo_6O_{19}]^{2-}$: (*a*) H. R. Allcock, E. C. Bissell and E. T. Shawl, *J. Am. Chem. Soc.*, 1972, **94**, 8603; (*b*) H. R. Allcock, E. C. Bissell and E. T. Shawl, *Inorg. Chem.*, 1973, **12**, 2963; (*c*) I. Lindqvist, *Ark. Kemi*, 1952, **5**, 247; (*d*) J. F. Keggin, *Nature*, 1933, **131**, 908; (*e*) B. Dawson, *Acta Crystallogr.*, 1953, **6**, 113; (*f*) J. S. Anderson, *Nature*, 1937, **140**, 850.

16 (*a*) A. Müller, E. Beckmann, H. Bögge, M. Schmidtmann and A. Dress, *Angew. Chem., Int. Ed.*, 2002, **41**, 1162; (*b*) A. Müller, S. K. Das, H. Bögge, C. Beugholt and M. Schmidtmann, *Chem. Commun.*, 1999, 1035; (*c*) A. Müller, P. Kögerler and C. Kuhlmann, *Chem. Commun.*, 1999, 1347; (*d*) P. Gouzerh and M. Che, *Actual. Chim.*, 2006, **298**, 9.

17 (*a*) I. V. Kozhevnikov, *Chem. Rev.*, 1998, **98**, 171; (*b*) I. V. Kozhevnikov, *J. Mol. Catal. A: Chem.*, 2007, **262**, 86.

18 (*a*) N. Mizuno and M. Misono, *Chem. Rev.*, 1998, **98**, 199; (*b*) N. M. Okun, T. Anderson and C. L. Hill, *J. Mol. Catal. A: Chem.*, 2003, **197**, 283; (*c*) K. Kamata, K. Yonehara, Y. Sumida, K. Yamaguchi, S. Hikichi and N. Mizuno, *Science*, 2003, **300**, 964; (*d*) A. M. Khenkin and R. Neumann, *J. Am. Chem. Soc.*, 2002, **124**, 4198; (*e*) E. F. Kozhevnikova and I. V. Kozhevnikov, *J. Catal.*, 2004, **224**, 164.

19 (*a*) C. L. Hill, L. Delannoy, D. C. Duncan, I. A. Weinstock, R. F. Renneke, R. S. Reiner, R. H. Atalla, J. W. Han, D. A. Hillesheim, R. Cao, T. M. Anderson, N. M. Okun, D. G. Musaev and Y. V. Geletii, *C. R. Chim.*, 2007, **10**, 305; (*b*) C. L. Hill, *J. Mol. Catal. A: Chem.*, 2007, **262**, 2.

20 (*a*) M. V. Vasylyev and R. Neumann, *J. Am. Chem. Soc.*, 2004, **126**, 884; (*b*) M. Vasylyev, D. Sloboda-Rozner, A. Haimov, G. Maayan and R. Neumann, *Top. Catal.*, 2005, **34**, 93; (*c*) R. Neumann and A. M. Khenkin, *Chem. Commun.*, 2006, 2529.

21 (*a*) J. T. Rhule, C. L. Hill and D. A. Judd, *Chem. Rev.*, 1998, **98**, 327; (*b*) B. Hasenknopf, *Front. Biosci.*, 2005, **10**, 275; (*c*) T. Yamase, *J. Mater. Chem.*, 2005, **15**, 4773.

22 I. A. Weinstock, *Chem. Rev.*, 1998, **98**, 113.

23 M. Sadakane and E. Steckhan, *Chem. Rev.*, 1998, **98**, 219.

24 C. R. Sprangers, J. K. Marmon and D. C. Duncan, *Inorg. Chem.*, 2006, **45**, 9628.

25 D.-L. Long, E. Burkholder and L. Cronin, *Chem. Soc. Rev.*, 2007, **36**, 105.

26 H. N. Miras, D.-L. Long, P. Kögerler and L. Cronin, *Dalton Trans.*, 2008, 214.

27 D. K. Walanda, R. C. Burns, G. A. Lawrance and E. I. von Nagy-Felsobuki, *Inorg. Chem. Commun.*, 1999, **10**, 487.

28 (*a*) F. Sahureka, R. C. Burns and E. I. von Nagy-Felsobuki, *J. Am. Soc. Mass Spectrom.*, 2001, **10**, 1136; (*b*) C. A. Ohlin, E. M. Villa, J. C. Fettinger and W. H. Casey, *Angew. Chem., Int. Ed.*, 2008, **47**, 1.

29 (*a*) D. K. Walanda, R. C. Burns, G. A. Lawrance and E. I. von Nagy-Felsobuki, *J. Chem. Soc., Dalton Trans.*, 1999, 311; (*b*) E. C. Alyea, D. Craig, I. Dance, K. Fisher, G. Willett and M. Scudder, *CrystEngComm*, 2005, **7**, 491.

30 D. K. Walanda, R. C. Burns, G. A. Lawrance and E. I. von Nagy-Felsobuki, *J. Cluster Sci.*, 2000, **1**, 5.

31 M. Bonchio, O. Bortolini, V. Conte and A. Sartorel, *Eur. J. Inorg. Chem.*, 2003, **4**, 699.

32 C. Boglio, G. Lenoble, C. Duhayon, B. Hasenknopf, R. Thouvenot, C. Zhang, R. C. Howell, B. P. Burton-Pye, L. C. Francesconi, E. Lacote, S. Thorimbert, M. Malacria, C. Afonso and J. C. Tabet, *Inorg. Chem.*, 2006, **3**, 1389.

33 (*a*) C. R. Mayer, C. Roch-Marchal, H. Lavanant, R. Thouvenot, N. Sellier, J. C. Blais and F. Sécheresse, *Chem.–Eur. J.*, 2004, **21**, 5517; (*b*) C. Dablemont, A. Proust, R. Thouvenot, C. Afonso, F. Fournier and J.-C. Tabet, *Inorg. Chem.*, 2004, **43**, 3514.

34 F. Sahureka, R. C. Burns and E. I. von Nagy-Felsobuki, *Inorg. Chem. Commun.*, 2002, **5**, 23.

35 M. J. Deery, O. W. Howarth and K. R. Jennings, *J. Chem. Soc., Dalton Trans.*, 1997, 4783.

36 R. Colton and J. C. Traeger, *Inorg. Chim. Acta*, 1992, **201**, 153.

37 J. L. Tuoi and E. Muller, *Rapid Commun. Mass Spectrom.*, 1994, **9**, 692.

38 T. Lau, J. Wang, R. Guevremont and K. Siu, *J. Chem. Soc., Chem. Commun.*, 1995, 877.

39 (*a*) T. Waters, R. A. J. O'Hair and A. G. Wedd, *J. Am. Chem. Soc.*, 2003, **125**, 3384; (*b*) T. Waters, R. A. J. O'Hair and A. G. Wedd, *Int. J. Mass Spectrom.*, 2003, **228**, 599; (*c*) J. Gun, A. Modestov, O. Lev, D. Saurenx, M. A. Vorotyntsev and R. Poli, *Eur. J. Inorg. Chem.*, 2003, **3**, 482.

40 (*a*) J. Shiea, W.-S. Wang, C.-H. Wang, P.-S. Chen and C.-H. Chou, *Anal. Chem.*, 1996, **68**, 1062; (*b*) J. Kim, Y. Dong, E. Larka and L. Que, Jr, *Inorg. Chem.*, 1996, **35**, 2369; (*c*) C.-H. Wang, M.-W. Huang, C.-Y. Lee, H.-L. Chei, J.-P. Huang and J. Shiea, *J. Am. Soc. Mass Spectrom.*, 1998, **9**, 1168; (*d*) S. Sakamoto, M. Fujita, K. Kim and K. Yamaguchi, *Tetrahedron*, 2000, **56**, 955.

41 K. Saito, Y. Sei, S. Miki and K. Yamaguchi, *Toxicon*, 2008, **51**, 1496.

42 M. Kunimura, S. Sakamoto and K. Yamaguchi, *Org. Lett.*, 2002, **4**, 347.

43 S. Sakamoto, M. Yoshizawa, T. Kusukawa, M. Fujita and K. Yamaguchi, *Org. Lett.*, 2001, **3**, 1601.

44 S. J. Park, D. M. Shin, S. Sakamoto, K. Yamaguchi, Y. K. Chung, M. S. Lah and J.-L. Hong, *Chem.–Eur. J.*, 2005, **11**, 235.

45 It should be noted that, when using both the techniques of ESI-MS and CSI-MS, the determined concentration of sensitive species (*i.e.* sensitive to changes in pH or the presence of other species) can still differ to some extent from that determined in bulk measurements. This effect was investigated by Howarth *et al.* during ESI-MS studies,[34] and is due to the interference in the equilibrium process by the drying agent (*e.g.* nitrogen gas) as the desolvation rapidly affects the pH and the concentrations of the solutes in the formation of the analytes.

46 Y. Jeannin and J. Martin-Frère, *Inorg. Chem.*, 1979, **18**, 3010.

47 Y. Ozawa and Y. Sasaki, *Chem. Lett.*, 1987, **185**, 923.

48 D. Rodewald and Y. Jeannin, *C. R. Acad. Sci., Ser. IIc: Chim.*, 1999, **2**, 3.

49 C. P. Pradeep, D.-L. Long, P. Kögerler and L. Cronin, *Chem. Commun.*, 2007, 4254.

50 H. N. Miras, D. J. Stone, E. J. L. McInnes, R. G. Raptis, P. Baran, G. I. Chilas, M. P. Sigalas, T. A. Kabanos and L. Cronin, *Chem. Commun.*, 2008, 4703.

51 (*a*) M. J. Manos, H. N. Miras, V. Tangoulis, J. D. Woolins, A. M. Z. Slawin and T. A. Kabanos, *Angew. Chem., Int. Ed.*, 2003, **42**, 425; (*b*) H. N. Miras, R. G. Raptis, P. Baran, N. Lalioti, M. P. Sigalas and T. A. Kabanos, *Chem.–Eur. J.*, 2005, **11**, 2295; (*c*) G. I. Chilas, H. N. Miras, M. J. Manos, J. D. Woollins, A. M. Z. Slawin, M. Stylianou, A. D. Keramidas and T. A. Kabanos, *Pure Appl. Chem.*, 2005, **9**, 1529; (*d*) H. N. Miras, R. G. Raptis, P. Baran, N. Lalioti, A. Harrison and T. A. Kabanos, *C. R. Chim.*, 2005, **8**, 957.

52 (*a*) H. N. Miras, J. D. Woollins, A. M. Slawin, R. Raptis, P. Baran and T. A. Kabanos, *Dalton Trans.*, 2003, 3668; (*b*) D.-L. Long, P. Kögerler and L. Cronin, *Angew. Chem., Int. Ed.*, 2004, **43**, 1817; (*c*) D.-L. Long, H. Abbas, P. Kögerler and L. Cronin, *Angew. Chem., Int. Ed.*, 2005, **44**, 3415.

53 C. Ritchie, E. M. Burkholder, D.-L. Long, D. Adam, P. Kögerler and L. Cronin, *Chem. Commun.*, 2007, 478.

54 C. P. Pradeep, D.-L. Long, G. N. Newton, Y.-F. Song and L. Cronin, *Angew. Chem., Int. Ed.*, 2008, **23**, 4388.

55 S. T. Zheng, Y. M. Chen, J. Zhang, J. Q. Xu and G. Y. Yang, *Eur. J. Inorg. Chem.*, 2006, **2**, 397.
56 H. Abbas, A. L. Pickering, D.-L. Long, P. Kögerler and L. Cronin, *Chem.–Eur. J.*, 2005, **4**, 1071.
57 E. F. Wilson, H. Abbas, B. J. Duncombe, C. Streb, D.-L. Long and L. Cronin, *J. Am. Chem. Soc.*, 2008, **130**, 13876.
58 B. M. Gatehouse and P. Leverett, *J. Chem. Soc., Dalton Trans.*, 1976, 1316.
59 Q. Li, P. F. Wu, Y. Xia, Y. G. Wei and H. Y. Guo, *J. Organomet. Chem.*, 2006, **691**, 1223.
60 M. Rancan, G. N. Newton, C. A. Muryn, R. G. Pritchard, G. A. Timco, L. Cronin and R. E. P. Winpenny, *Chem. Commun.*, 2008, 1560.
61 (*a*) P. J. Kitson, Y.-F. Song, P. Gamez, P. de Hoog, D.-L. Long, A. D. C. Parenty, J. Reedijk and L. Cronin, *Inorg. Chem.*, 2008, **47**, 1883; (*b*) A. D. C. Parenty, L. V. Smith, A. L. Pickering, D.-L. Long and L. Cronin, *J. Org. Chem.*, 2004, **69**, 5934; (*c*) A. D. C. Parenty, L. V. Smith, K. M. Guthrie, D.-L. Long, J. Plumb, R. Brown and L. Cronin, *J. Med. Chem.*, 2005, **48**, 4504.